Published in final edited form as:
J Phys Chem B. 2010 July 22; 114(28): 9165–9172. doi:10.1021/jp1039942.

A Molecular Dynamics Study of the Behavior of Selected Nanoscale Building Blocks in a Gel-Phase Lipid Bilayer

Patrick S. Redmill[1] and **Clare McCabe**[1,2,*]

[1] Department of Chemical and Biomolecular Engineering, Vanderbilt University, Nashville, TN 37235, USA

[2] Department of Chemistry, Vanderbilt University, Nashville, TN 37235, USA

Abstract

The cellular membrane functions as a regulating barrier between the intracellular and extracellular regions. For a molecule to reach the interior of the cell from the extracellular fluid, it must diffuse across the membrane, via either active or passive transport. The rigid structure of lipid bilayers, which are a key component of cellular membranes, prohibit simple diffusion of most particles, while vital nutrients are transported to the interior by specific mechanisms, such as ion channels and transport proteins. Although the cellular membrane provides the cell with protection against unwanted toxins that may be in the extracellular medium, some foreign particles can reach the interior of the cell, resulting in irregularities in cellular function. This behavior is particularly noted for permeants with compact molecular structure, suggesting that common nanoscale building blocks, such as fullerenes, may enter into the interior of a cell. To gauge the propensity for such particles to cross the membrane, we have computed the Gibbs free energy of transfer along the axis normal to the bilayer surface for two nanoscale building blocks, C_{60} and a hydrogen-terminated polyhedral oligomeric silsequioxane (H-POSS) monomer, in a hydrated dipalmitoylphosphatidylcholine (DPPC) bilayer using molecular dynamics simulations and potential of mean force calculations. The studies show that C_{60} has a substantial energetic preference for the soft polymer region of the lipid bilayer system, below the water/bilayer interface, with a transition energy from bulk water of −19.8 kcal/mol. The transition of C_{60} from the bulk water to the center of the bilayer, while also energetically favorable, has to overcome a +5.9 kcal/mol energetic barrier in the hydrophobic lipid tail region. The H-POSS simulations indicate an energy minimum at the water-bilayer interface, with an energy of −10.9 kcal/mol; however, a local minimum of −2.7 kcal/mol is also observed in the hydrophobic dense-aliphatic region. The energy barrier seen in the hydrophobic core region of the C_{60} study is likely due to the significant penalty associated with inserting the relatively large particle into such a dense region. In contrast, while H-POSS is found to be subject to an energetic penalty upon insertion into the bilayer, the relatively small size of the H-POSS solute renders this penalty less significant. The energy barrier seen in the soft polymer region for the H-POSS monomer is primarily attributed to the lack of favorable solute-bilayer electrostatic interactions, which are present in the interfacial region, and fewer van der Waals interactions in the soft polymer region than the dense aliphatic region. These results indicate that C_{60} may partition into the organic phase of the DPPC/water system, given the favorable free energies in the soft polymer and dense aliphatic regions of the bilayer, while H-POSS is likely to partition near the water-bilayer interface, where the particle has low-energy electrostatic interactions with the polar head groups of the bilayer.

*Corresponding author. Phone: 615 322-6853. Fax: 615 343-7951. c.mccabe@vanderbilt.edu.

Keywords

DPPC; fullerene C_{60}; POSS; nanoparticle; molecular dynamics; potential of mean force; Gibbs free energy; solubility

Introduction

Many toxins act by attacking biological systems at a cellular level and disrupting cellular structure or function, resulting in apoptosis (programmed cell death) or necrosis (abnormal cell death). Toxins can, for example, alter the structure of the cellular membrane, resulting in cell wall loosening and rupture (i.e., cell lysis)[1] or enter the intercellular region and induce abnormal cell function, such as increased mitochondrial function or ATP production, [2] inducing apoptosis. Toxins often access the cell via active transport or facilitated diffusion, by mechanisms such as ion channel permeation[3] or binding with transport proteins,[4] while some small particles exhibit appreciable passive diffusion without the aid of such transport mechanisms.[5,6]

Partitioning of solutes into a lipid bilayer is a complex process influenced in large part by energetic considerations. By comparing the free energy of solvation in organic and water phases, qualitative conclusions about the partitioning of particles between aqueous/organic phases can be made, which by extension can provide some insight into the fate of the particles in analogous systems, such as soil/water[7] and tissue/water systems.[8] A common parameter used to quantify organic/aqueous partitioning is the octanol-water partition coefficient ($K_{O/W}$); however, $K_{O/W}$ coefficients describing partitioning of a molecule between an aqueous phase and an isotropic organic phase, such as octanol, may be insufficient to describe the partitioning between an aqueous phase and an anisotropic, semi-ordered organic phase, such as a phospholipid membrane. Additionally, complex membrane systems exhibit several different structural phases, which have significant effects on solute partitioning, over relatively small ranges of conditions.[9] For example, the partitioning of benzene in dimyristoylphosphatidylcholine (DMPC) model bilayer systems decreases by an order of magnitude when the temperature is lowered below the gel-phase transition temperature of 23.5 °C.[10,11] In contrast, the partitioning of benzene in an octanol/water system only changes by 2.5% when the temperature is lowered from 25 °C to 15 °C.[12]

In light of the growing interest in incorporating nanoparticles into biological systems for various applications, ranging from diagnostics (such as MRI contrasting agents)[13] to therapeutics and drug delivery,[14–17] the determination of their toxic potential has become a key issue. The particles considered in this study (Figure 1), which were chosen due to their compact size and highly symmetric shape, have been proposed as nanoscale building blocks (NBBs) for many applications, thus significantly increasing the likelihood of occupational, environmental and biological exposure to these nanoparticles. For example, functionalized versions of the nanoparticles in Figure 1 have been proposed as possible HIV protease inhibitors,[18] light-mediated DNA cleaving agents,[19] dental restorative composites,[20] and vascular prostheses.[21] Recent studies have suggested that these nanoparticles may exhibit some toxic traits. In particular, evidence suggests that buckyballs cause oxidative stress in the brain tissue of juvenile large mouth bass,[22] can potentially bind to and deform DNA fragments,[23] and partition significantly in the organic phase of octanol/water systems,[24] while a cationic variant of the POSS molecule has been shown to be able to diffuse across the cellular membrane and gain access to the cytosol,[25] where it has the potential to interfere with intracellular processes.

In an effort to develop a more fundamental understanding of nanoparticle-bilayer interactions both experimental[26,27] and theoretical[28–32] studies have begun to examine the fate of nanoparticles in model bilayer systems, focusing in particular on the C_{60} fullerene. A DPPC bilayer is generally used in these model studies, since human cell membranes are typically comprised of over 90% phospholipids, of which 60% is DPPC.[33] As a result DPPC has been extensively studied and can be considered both experimentally and computationally as the benchmark lipid in the study of model bilayers.[34] Both experimental and theoretical studies indicate that C_{60} will partition into the interior of a liquid crystalline phase phospholipid bilayer, and generally all agree that the partitioning is largely due to the fact that the hydrophobic C_{60} particle is in a high-energy state when solvated in the aqueous phase compared to a relatively low-energy state when found in the ordered hydrocarbon interior of the bilayer, resulting in an energetic minimum occurring in the hydrocarbon chain region. Amongst the theoretical studies, which focus on free energy calculations using constraint molecular dynamics as in the current work, whilst there is agreement that the C_{60} particle energetically favors the interior hydrocarbon region of the phospholipid bilayer, there is disagreement concerning the magnitude and location of the minimum energy (defined in terms of the distance away from the center of the bilayer). We note however that between each of the prior simulation studies there are significant differences, including the use of coarse-grained as opposed to atomistically detailed models, differences in the parameterization techniques for the force fields used, and differences in the system parameters, including system size and frequency of sampling. Here we briefly summarize the findings of these earlier studies as they pertain to the current work.

In the fully atomistic DPPC bilayer study of Qiao *et al.*[28] a relatively small well depth of −8.3 kcal/mol was observed, whereas the coarse-grained DPPC study of D'Rozzario *et al.*[30] indicated a considerably larger well depth of −47.5 kcal/mol. In contrast, the coarse-grained work of Wong and Ekkabut[31] and the fully atomistic simulations of Bedrov *et al.*[29] are in general agreement, with energetic well depths of approximately −25 kcal/mol (−26.3 kcal/mol in the coarse-grained DPPC bilayers studied by Wong and −22 kcal/mol in the atomistic DMPC bilayer of Bedrov) reported. The energetically preferable distance predicted by Bedrov and coworkers was between 6 − 7Å[29] from the center of the bilayer, whereas the studies of Qiao *et al.* and Wong-Ekkabut *et al.* indicate that the energy minimum is approximately 10Å from the center of the bilayer, while D'Rozzario et al. indicate an energy minimum at the bilayer center. Additionally, in both the simulations reported by Qiao[28] and coworkers and by Bedrov[29] and coworkers, a very slight energetic barrier was found at the center of the bilayer. In contrast, in both coarse-grained studies[30,31] no significant energetic barrier in the interior of the bilayer was found, indicating that C_{60} may easily reach the center of the bilayer.

In this work, the Gibbs free energy required to insert nanoparticles at various depths normal to the bilayer plane (hitherto referred to as the *z* direction), ($\Delta G(z)$), has been calculated in a fully hydrated DPPC (Figure 2) bilayer using molecular dynamics simulations and potential of mean force calculations. The simulations were carried out at 298 K and 1 atm under conditions at which the DPPC bilayer is in the gel-phase, in contrast to previous studies, which were all in the liquid crystalline phase. While phospholipid bilayers in biological systems are predominantly in the liquid-crystalline phase, it has been acknowledged that many biological membranes consist of multiple phospholipids phases,[9,35] and that the densely packed gel-phase typically suppresses diffusion across the membrane. The calculated $\Delta G(z)$ profiles describe the partitioning behavior of each nanoparticle in the bilayer and therefore provide insight into the thermodynamic driving force and ability of a C_{60} or H-POSS molecule to partition into biological membranes.

Simulation Details

Molecular dynamics simulations have been performed and potential of mean force calculations used to determine the *z* -directed Gibbs free energy $\Delta G(z)$ for C_{60} and H-POSS molecules in a fully hydrated DPPC bilayer. Bilayer systems are commonly separated into 4 distinct groups along the heterogeneous *z* axis[36,34] as shown in Figure 3. Region 1 is the so-called "perturbed water" region that encompasses the depth from approximately 8Å above the bilayer surface (at which point the water structure is that of bulk water), to the depth where the lipid and water densities become equal. Region 2, the "interfacial" region, is characterized by a dramatic drop in water density and is comprised primarily of DPPC choline and phosphate groups. Region 3 is the "soft polymer" region, which is represented by a steady rise in hydrocarbon density and continues to a depth of ~13Å from the center of the membrane. Region 4 is the hydrophobic region and exhibits a very high, crystalline-like structure due to the ordering of the hydrocarbon tails up to a depth of about 6Å from the center of the bilayer, where a substantial drop in hydrocarbon density is observed.

The overall resistance (R) associated with solute permeation crossing a heterogeneous bilayer of depth d, defined as the inverse of the permeability coefficient (P), is connected to the diffusivity function, $D(z)$, and $\Delta G(z)$ through the following relations [37]

$$R=\frac{1}{P}=\int_0^d \frac{dz}{K(z)D(z)} \tag{1}$$

$$K(z)=e^{\frac{-\Delta G(z)}{RT}} \tag{2}$$

where $K(z)$ is the lipid/water partitioning function and describes the ratio of the concentration of solute in the lipid and the water phases. The $\Delta G(z)$ function can be obtained by performing a potential of mean force study on the solutes over each of the four regions in Figure 3. The potential of mean force calculation is performed by fixing the center of mass of the solute at a given *z* -depth of the bilayer; the molecule is able to freely translate in the *x* and *y* directions and individual atoms on the solute can move along the *z*-axis. The forces acting upon individual atoms in the solute can be calculated and used to determine the force on the center of mass ($\mathbf{F}(z, t)$) required to keep the solute fixed at the chosen depth. The $\Delta G(z)$function is in turn obtained from,[38]

$$\Delta G(z)= -\int_{z_{ref}}^{z} \left\langle \mathbf{F}(z') \right\rangle dz' \tag{3}$$

where z_{ref} is the region from which the change in energy will be in reference to (in this study, taken as region 1 of Figure 3), and $\langle \cdots \rangle$ indicates an ensemble average. To simplify the calculation of $\langle \mathbf{F}(z, t) \rangle$, both the C_{60} and H-POSS structures were held rigid during the simulations by calculating the total force and torque on the particle, obtained from summing the forces and torques on its constituent atoms and updating the coordinates, velocities, and orientations of the atoms in a manner that moves and rotates the particle as a single body. This simplification is justified since both H-POSS[39–41] and C_{60}[42,43] have been shown to have somewhat rigid structures. Furthermore, treating the solutes as rigid molecules also greatly reduces the required sampling time, as it has been shown that solute flexibility necessitates longer sampling periods, particularly for large solutes[44] like those studied in

this work. The simulations were performed using the LAMMPS[45] molecular dynamics code, employing the particle-particle-particle mesh Ewald method for long-ranged interactions and a velocity-Verlet integrator with a 1 fs time step, a 8Å Lennard-Jones cutoff and a 10Å electrostatic real space cutoff.

In order to accurately model a membrane, either the surface area per lipid or the surface tension of the membrane must be known.[34] While there is considerable debate on the appropriate value of the water/DPPC membrane surface tension[46–49] the area per lipid is better defined;[34] therefore, the simulations were performed in the *NPAT* ensemble, in which the number of particles (*N*), the pressure normal to the bilayer (*P*), the cross sectional-area of the bilayer surface (*A*), and the temperature (*T*) are held constant. The simulations contained 288 DPPC molecules and 8375 water molecules, with an area per lipid of 47.2 $Å^2$/lipid at a system temperature of 298K.[50] Cavities for the nanoparticles were created by inserting spherical particles into the membrane system and growing the solute-solvent interactions from zero to the full interactions over a 150 ps time period; this approach minimizes the disruption of the bilayer due to the insertion of the particle and therefore reduces the subsequent equilibration time. This was accomplished by inserting a bead, approximately the size of the nanoparticles of interest, using the “expand” form of the standard Lennard-Jones pair potential, as implemented in LAMMPS.

$$U(r_{ij})=4\varepsilon\left[\left(\frac{\sigma}{r_{ij}-\Delta}\right)^{12}-\left(\frac{\sigma}{r_{ij}-\Delta}\right)^{6}\right]$$

The Δ term in equation 4 modifies the potential energy between the bead and the bilayer, such that Δ can be increased smoothly from −σ to 0 until a hole of sufficient size (i.e., of diameter σ) is present in the bilayer, at which point the explicit nanoparticle is inserted. It was found that inserting the nanoparticle into such a pre-established cavity in the bilayer enabled more rapid convergence of the potential energy of the entire system (compared to direct insertion of the nanparticle or allowing a disordered system to self-assemble around the solute). The systems were all equilibrated for 4 ns, followed by additional simulations of 4 ns during which the trajectories were sampled at 1 ps intervals.

It must be noted that the insertion of a large particle into a bilayer will result in a disruption in the local structure. Such disruptions include transiently stressing intramolecular properties of the bilayer, such as 3-body angles and dihedral angles. Additionally, unfavorable intermolecular interactions may arise between the membrane and the solute or interactions between lipid molecules, such as a disrupted hydrogen-bond network in the region where the particle was introduced. The temporary disruption of the membrane structure will effect the $\Delta G(z)$ calculation, therefore it is essential that sufficient equilibration is performed so that the bilayer is satisfactorily relaxed around the solute. Average force profiles were determined and indicate that the forces on the solute are satisfactorily converged in the 4 ns equilibration period.

The CHARMM27 force field[51] was used to model the hydrated phospholipid system with the standard TIP3P[52] force field to describe the water molecules. To model the C_{60} molecule we used the van der Waals parameters for aromatic carbons in the CHARMM27 force field. For H-POSS, the water-silica force field of Cruz-Chu *et al.* was used.[53] This force field was chosen due to the fact that it is the only silicon-based force field parameterized for the use with the CHARMM force field and has been shown to reproduce wetting characteristics of water on a silica surface, a phenomena that strongly correlates to the Gibbs free energy of solvation.[54] Additionally, this force field is based upon the GLASSFF force field,[55] which

has been shown to exhibit superior bulk nanoparticle energies, structures, thermal stability, and surface interactions as compared to other common silicon-based force fields, such as Tsuneyuki-Tsukada-Aoki-Matsui (TTAM)[56] and the van Beest-Kramer-van Santen (BKS)[57] force fields. While the GLASSFF force field was fitted using DFT cluster energies for POSS-like particles, partial charge information for H-POSS, in particular, is unavailable. Partial atomic charges for H-POSS were therefore obtained using a Mulliken population analysis from a B3LYP-DFT/6-311G** point energy calculation with a structure obtained from a B3LYP-DFT/6-31G geometry optimization on an isolated H-POSS molecule. Geometry and partial charge information for H-POSS are provided in Tables 1 and 2. The *ab initio* studies were performed using NWCHEM.[58]

Results and Discussion

As discussed above, the energetic behavior of the particles along the heterogeneous axis of a DPPC bilayer has been calculated. A 2 ns molecular dynamics simulation of an unperturbed hydrated DPPC bilayer was first performed to confirm that the simulated model bilayer is consistent with those used in earlier simulation studies.[36] In Figure 4 we present density profiles for pertinent atom groups in the unperturbed DPPC bilayer and note that the density profiles are similar to those reported for liquid crystalline DPPC bilayers.[34,59,60] The main differences between the gel-phase profile in figure 4 and the liquid-crystalline phase profiles, is that the gel-phase is elongated along the z-axis, due to the decreased area per lipid, and the gel-phase bilayer exhibits a higher degree of structure, particularly in the hydrophobic region. Figure 4 reflects the characteristics of each region as described in the four-region model: namely, the system approaches a density consistent with that of pure water around 29Å away from the center of the bilayer (at the interface of regions 1 and 2); a significant presence of polar heads is observed between the depths of 21Å – 29Å (region 2); a relatively low density, yet increasingly structured region of hydrocarbon chains is seen between 13Å – 21Å (region 3); a highly structured hydrocarbon region from 6Å – 13Å (region 4); and a relatively low density aliphatic region in the center of the bilayer.

Study of C_{60} in DPPC

The calculated $\Delta G(z)$ function for the C_{60} particle along the heterogeneous axis of the gel-phase DPPC bilayer studied is presented in Figure 5. From the figure it can be seen that, as in previous studies, the water phase is found to be a very high-energy region for C_{60} relative to the hydrocarbon regions of the DPPC membrane. This is not surprising given the well-documented hydrophobicity of C_{60}. The free energy is seen to drop significantly as the C_{60} moves from region 1 (Figure 3) towards the bilayer interface (region 2) i.e., from distances of approximately 26 – 22Å, as confirmed by the profiles presented in Figure 4. In this region of the bilayer, it is likely that the dense hydrogen-bonded structure of water will be disrupted by the presence of the bilayer, therefore providing more free volume to the solute, resulting in a smaller energy penalty for creating the cavity to accommodate the particle. Additionally, although energetic penalties would be incurred for disrupting the electrostatic interactions between the polar heads of the phospholipids, the nitrogen in the head group is rich in methyl groups, which would exhibit favorable interactions with the carbon-based C_{60}.

As expected, the energetic minimum for C_{60} is found in the predominantly hydrocarbon-rich region (region 3) of the phospholipid bilayer, at 18Å from the bilayer center. The Gibbs free energy of transfer from the water region, to this depth is −19.8 kcal/mol, indicating a relatively strong affinity for the region between the interfacial (region 2) and soft-polymer (region 3) regions. In agreement with the study of liquid crystalline DPPC membranes by Qiao et al.,[28] the energy profile is seen to increase as the C_{60} moves from the soft polymer region (region 3) to the hydrophobic region (region 4) towards the center of the bilayer. This

increase in energy is likely due to the increase in density of the hydrocarbon chains as the center of the bilayer is approached, which is particularly pronounced in the gel-phase. The increase in hydrocarbon density in region 4, due to the ordering of the DPPC tails, will limit the available free volume and result in a greater energy penalty for the creation of the cavity into which the particle is inserted. Additionally, although the high carbon density on the surface of C_{60} will result in favorable van der Waals interactions between the C_{60} and the hydrocarbon chains, as noted by Bedrov et al.,[29] it seems likely that this energy gain will be outweighed by the energy penalty due to the creation of the C_{60} sized cavity in the dense hydrocarbon medium. We note that the studies of Bedrov et al.[29] and D'Rozzario et al.[30] find much smaller, or non-existent energy barriers, in the hydrophobic region of the liquid crystalline membrane. However, one would expect the energy penalty due to cavity creation in a gel-phase bilayer (which has considerably less free volume than that of the liquid crystalline bilayer) to be higher. This could explain the observed differences. Additionally, in the case of D'Rozzario et al.,[30] the coarse-grained nature of the work may have prevented observing the subtle energy barrier seen by Bedrov et al.[29] We also note that the energy minimum in this work is deeper than the well depth value of −8.3 kcal/mol reported by Qiao et al., but comparable to the value of −22 kcal/mol reported by Bedrov *et al*.[29] We speculate that the energy minimum observed in this work is further from the center of the bilayer due to the more ordered nature of the gel-phase bilayer compared to the liquid crystalline bilayer studied in other work. Inserting the C_{60} closer to the center of the membrane in a denser hydrocarbon zone would result in a situation where the energy due to cavity creation outweighs the contribution from enhanced van der Waals interactions, which is consistent with the substantial energy barrier observed.

The relatively large energy difference between the center of the bilayer and the soft-polymer region (region 3) indicates that C_{60} will likely partition into the soft polymer region of the gel-phase lipid bilayer and will have trouble reaching the interior of the membrane. Although permeation through a gel-phase membrane has not been studied in the literature, the partitioning behavior of several, smaller molecules in a variety of phospholipids bilayer phases has been studied.[61–63] Benzene, for example, is found to exhibit a decrease in membrane/water partitioning of an order of magnitude over the liquid crystalline to gel phase transition.[10,11] Therefore, given the relative size of C_{60}, the significant change in partitioning behavior between the liquid crystalline and gel phases is reasonable.

In an effort to better understand the migration of the C_{60} particle, a MD simulation of a free floating C_{60} particle, initialized in the soft polymer region, consisting of a 2 ns equilibration run and a 2 ns sampling run was performed. Similar studies initiating the C_{60} in the water phase and observing the diffusion through a liquid crystalline membrane have been reported in the literature using atomistic[28] and coarse-grained[31] force fields. Both studies show that C_{60} diffuses through the membrane, however, the atomistic study of Qiao et al.[28] indicates a required time of 48 ns, while the coarse-grained study of Wong-Ekkabut and coworkers[31] indicates a relatively short diffusion time of 500 ps. While we do not hope to study C_{60} translocation, we can sample the probability density of C_{60} occupying different depths in the vicinity of the interfacial region, as shown in Figure 6. The results indicate that C_{60} translates very minimally at the interface, with the particle predominantly occupying the region between 22Å – 25Å from the center of the bilayer. This suggests that both the aliphatic region of the membrane and the bulk water region exert significant competing forces on the particle, likely resulting in a lessened probability of finding the C_{60} in either the water phase or bilayer core. The probability distribution indicates that C_{60} is most likely found at around 23.5Å from the bilayer center. While both the potential of mean force and free-floating studies suggest that C_{60} will ultimately partition into the soft polymer region of the membrane, in the free-floating studies the C_{60} does not settle directly at the depth of the energy minimum at 18Å, but rather near the local hydrocarbon density maximum of 22.5 Å

shown in Figure 4. The particle will be largely segregated from the water at this depth and will be in contact with the alkane tail and polar head regions of the bilayer (region 2). The fact that C_{60} never fully enters the water phase further suggests that there is an energetic preference for the C_{60} to embed into the organic material in the system, as opposed to the water region. In the case of a C_{60} molecule that can translate along the z-axis, it is reasonable to expect that the structure of the hydrocarbon tails around the hydrocarbon density maxima will be disrupted by the movement of such a large particle through a generally rigid region of the membrane, thereby increasing the free volume in this region. It is likely that, over longer time-scales, the membrane structure will relax, limiting the movement of the particle, and ultimately *pushing* it to the depth at which the energy minima occurs.

Study of H-POSS in DPPC

The $\Delta G(z)$ function for the H-POSS particle along the heterogeneous axis of the DPPC bilayer studied is presented in Figure 7. Figure 7 shows that H-POSS energetically prefers the interfacial region of the bilayer, with a Gibbs free energy of transfer from the water region of −10.9 kcal/mol at a depth of 22 Å from the bilayer center; however, the figure also shows a local minima in the hydrophobic region with $\Delta G = -2.7$ kcal/mol at 8 Å away from the bilayer center. The minima seen in the hydrophobic region for the H-POSS system is likely due to the increase in favorable solute-bilayer van der Waals interactions, which are a result of the denser packing of the aliphatic tails in this region. It should be noted that while H-POSS will be subject to an energetic penalty due to the insertion of the particle in this dense region, similar to that seen for C_{60}, given the relatively small size of H-POSS this penalty will be less significant. The significant global minima near the polar head region is likely due to the favorable electrostatic interactions between the charged H-POSS monomer and the polar heads of the DPPC bilayer. The energy barrier occurring between these two regions is a result of the soft polymer region lacking the favorable electrostatic interactions characteristic of the interfacial area and the high density of the hydrophobic core, resulting in fewer low-energy van der Waals interactions with the bilayer. Given the deep energy well at 22 Å and the considerable energy barrier in the soft-polymer region, it seems likely that the H-POSS monomer will partition to the interfacial region of the bilayer.

As with C_{60}, a 2 ns simulation of a free floating H-POSS molecule in the DPPC membrane was performed following a 2 ns equilibration period. The position of the H-POSS was initialized in the soft polymer region, at a depth of approximately 18Å. In Figure 8 we present the probability density of H-POSS occupying various depths of the bilayer. H-POSS, like C_{60}, remains underneath the water/membrane interface at depths of 20–24Å, with the profile exhibiting a maximum at 22.5Å. In this case, the free floating simulation indicates essentially the same preferential depth as the potential of mean force study and therefore supports the findings that H-POSS will likely partition into the soft-polymer region of the bilayer, near the polar head groups of the membrane.

Conclusions

The Gibbs free energy for C_{60} and H-POSS nanoparticles crossing a gel-phase DPPC bilayer has been calculated using constraint dynamics molecular dynamics simulations. Additionally, free-floating simulations of both particles have been performed in an effort to clarify the partitioning behavior of the particles in interfacial regions. It was found that C_{60} preferentially partitions into the organic phase of a hydrated DPPC system, whereas H-POSS is likely to be found at the water-bilayer interface.

The C_{60} particle exhibits an energy minimum in the relatively low-density soft polymer region of DPPC, due in large part to the increased van der Waals interactions with the

aliphatic tails and relatively large free volume available to the solute. The interior of the gel phase of the DPPC membrane provides relatively little free volume available to C_{60}, therefore, although the interior of the membrane has more low-energy van der Waals interactions available to the solute, the structure of the aliphatic chains is too rigid to allow the partitioning from the shallow interfacial/soft polymer region (region 3) to the interior of the membrane (region 4) due to the significant energetic penalty due to the insertion of the particle in the densely packed region.

For H-POSS the simulation results show two energy minima across the heterogeneous bilayer axis, with a local minima occurring in the hydrophobic region (region 4) and a global minima occurring at the water bilayer interface (region 2). An energetic penalty of +15.0 kcal/mol was noted for transferring H-POSS from the depth of 22Å to 16Å. The energy minima seen at the interface is likely due to enhanced electrostatic interactions between the polar head groups of the DPPC bilayer and the H-POSS monomer. Furthermore, the minima observed in the hydrophobic region of the bilayer can be attributed to the greater number of low energy van der Waals interactions available to the solute in the dense region in addition to a decreased penalty of insertion due to the relatively small size of the particle, compared to C_{60}.

The energy profiles observed for C_{60} and H-POSS in this study indicate that both particles may not completely partition into the interior of dense, gel-phase membranes, with transfer of the particle to the center of the bilayer corresponding to a significant energy penalty relative to the energetic minima. These results imply that C_{60} and H-POSS may not readily diffuse through a gel-phase bilayer, which may result in limited transport across biological membranes that contain gel-phase regions. The C_{60} results mirror similar studies in liquid crystalline phospholipid bilayer systems in that the energy minimum for both phases, are approximately −20 kcal/mol. Liquid crystalline studies however, indicate that the energy minimum occurs between 6 – 10Å from the center of the membrane, whereas the minimum distance in this study is around 18 Å. This difference is attributed to the denser inner core of the gel-phase system, for which a significant energy penalty would exist to create a cavity for the C_{60} particle due to a lack of free volume.

Acknowledgments

This research used resources of the National Energy Research Scientific Computing Center, which is supported by the Office of Science of the U.S. Department of Energy under Contract No. DE-AC02-05CH11231. PSR also gratefully acknowledge support from the National Science Foundation through grant CHE-0626259 and CMC the National Institute of Arthritis and Muscoskeletal and Skin Diseases through grant number R21 AR053270-02.

References

1. Yanganza ES, Rioux D, Simard M, Arul J, Tweddell RJ. Applied and Environmenal Microbiology. 2004; 70:6800.
2. Carranza-Rosales P, Said-Fernandez S, Sepulveda-Saavedra J, Cruz-Vega DE, Gandolfi AJ. Toxicology. 2005; 210:111. [PubMed: 15840425]
3. Levina A, Harris HH, Lay PA. J Biol Inorg Chem. 2006; 11:225. [PubMed: 16362419]
4. Devanathan S, Postle K. Molecular Microbiology. 2007; 65:441. [PubMed: 17578453]
5. Johnson ME, Berk DA, Blankschtein D, Golan DE, Jain RK, Langer RS. Biophysical Journal. 1996; 71:2656. [PubMed: 8913603]
6. Mitragotri S. Journal of Pharmaceutical Sciences. 2002; 91:744. [PubMed: 11920759]
7. Cronin MTD. Current Computer - Aided Drug Design. 2006; 2:405.
8. Lian GP, Chen LJ, Han LJ. Journal of Pharmaceutical Sciences. 2008; 97:584. [PubMed: 17722002]
9. Koynova R, Caffrey M. Biochemica et Biophysica Acta. 1998; 1376:910145.

10. Deyoung LR, Dill KA. Biochemistry. 1988; 27:5281. [PubMed: 3167046]
11. Deyoung LR, Dill KA. Journal of Physical Chemistry. 1990; 94:801.
12. Finizio A, Di Guardo A. Chemosphere. 2001; 45:1063. [PubMed: 11695583]
13. Frankamp BL, Fischer NO, Hong R, Srivastava S, Rotello VM. Chemistry of Materials. 2006; 18:956.
14. Bosi S, Da Ros T, Spalluto G, Prato M. European Journal of Medicinal Chemistry. 2003; 38:913. [PubMed: 14642323]
15. Chellat F, Merhi Y, Moreau A, Yahia L. Biomaterials. 2005; 26:7260. [PubMed: 16023200]
16. Yih TC, Al-Fandi M. Journal of Cellular Biochemistry. 2006; 97:1184. [PubMed: 16440317]
17. Murakami T, Tsuchida K. Mini-Reviews in Medicinal Chemistry. 2008; 8:175. [PubMed: 18289101]
18. Abbott AP, Eardley CA. Journal of Physical Chemistry B. 1999; 103:2504.
19. Tokuyama H, Yamago S, Nakamura E, Shiraki T, Sugiura Y. Journal of the American Chemical Society. 1993; 115:7918.
20. Fong H, Dickens SH, Flaim GM. Dental Materials. 2005; 21:520. [PubMed: 15904694]
21. Kannan RY, Salacinski HJ, De Groot J, Clatworthy I, Bozec L, Horton M, Butler PE, Seifalian AM. Biomacromolecules. 2006; 7:215. [PubMed: 16398518]
22. Oberdorster E. Environmental Health Perspectives. 2004; 112:1058. [PubMed: 15238277]
23. Zhao XC, Striolo A, Cummings PT. Biophysical Journal. 2005; 89:3856. [PubMed: 16183879]
24. Redmill PS, Capps SC, Cummings PT, McCabe C. Carbon. 2008 in press.
25. McCusker, C.; Carroll, JB.; Rotello, VM. Chemical Communications. 2005. p. 996
26. Chen YJ, Bothun GD. Langmuir. 2009; 25:4875. [PubMed: 19397348]
27. Jeng US, Hsu CH, Lin TL, Wu CM, Chen HL, Tai LA, Hwang KC. Physica B-Condensed Matter. 2005; 357:193.
28. Qiao R, Roberts AP, Mount AS, Klaine SJ, Ke PC. Nano Letters. 2007; 7:614. [PubMed: 17316055]
29. Bedrov D, Smith GD, Davande H, Li LW. Journal of Physical Chemistry B. 2008; 112:2078.
30. D'Rozario RSG, Wee CL, Wallace EJ, Sansom MSP. Nanotechnology. 2009; 20:7.
31. Wong-Ekkabut J, Baoukina S, Triampo W, Tang IM, Tieleman DP, Monticelli L. Nature Nanotechnology. 2008; 3:363.
32. Li Y, Chen X, Gu N. Journal of Physical Chemistry B. 2008; 112:16647.
33. Morrow MR, Temple S, Stewart J, Keough KMW. Biophysical Journal. 2007; 93:164. [PubMed: 17434940]
34. Tieleman DP, Marrink SJ, Berendsen HJC. Biochimica Et Biophysica Acta-Reviews on Biomembranes. 1997; 1331:235.
35. Subczynski WK, Wisniewska A. Acta Biochemica Polonica. 2000; 47:613.
36. Bemporad D, Luttmann C, Essex JW. Biochimica Et Biophysica Acta-Biomembranes. 2005; 1718:1.
37. Marrink SJ, Berendsen HJC. Journal of Physical Chemistry. 1994; 98:4155.
38. Kubo R. Reports on Progress in Physics. 1966; 29:255.
39. Chan ER, Striolo A, McCabe C, Cummings PT, Glotzer SC. Journal of Chemical Physics. 2007; 127:4102.
40. Ionescu TC, Qi F, McCabe C, Striolo A, Kieffer J, Cummings PT. Journal of Physical Chemistry B. 2006; 110:2502.
41. Li HC, Lee CY, McCabe C, Striolo A, Neurock M. Journal of Physical Chemistry A. 2007; 111:3577.
42. Lu X, Chen ZF. Chemical Reviews. 2005; 105:3643. [PubMed: 16218563]
43. Kroto HW. Nature. 1987; 329:529.
44. Wescott JT, Fisher LR, Hanna S. Journal of Chemical Physics. 2002; 116:2361.
45. Plimpton S. Journal of Computational Physics. 1995; 117:1.

46. Egberts E, Marrink SJ, Berendsen HJC. European Biophysics Journal with Biophysics Letters. 1994; 22:423. [PubMed: 8149924]
47. Feller SE, Pastor RW. Biophysical Journal. 1996; 71:1350. [PubMed: 8874010]
48. Jahnig F. Biophysical Journal. 1996; 71:1348. [PubMed: 8874009]
49. Chiu SW, Clark M, Balaji V, Subramaniam S, Scott HL, Jakobsson E. Biophysical Journal. 1995; 69:1230. [PubMed: 8534794]
50. Tu K, Tobias DJ, Blasie JK, Klein ML. Biophysical Journal. 1996; 70:595. [PubMed: 8789079]
51. Feller SE, MacKerell AD. Journal of Physical Chemistry B. 2000; 104:7510.
52. Jorgensen WL, Chandrasekhar J, Madura JD, Impey RW, Klein ML. Journal of Chemical Physics. 1983; 79:926.
53. Cruz-Chu ER, Aksimentiev A, Schulten K. Journal of Physical Chemistry B. 2006; 110:21497.
54. de Gennes, P-G.; Brochard-Wyatt, F.; Quéré, D. Capillarity and Wetting Phenomena: Drops, Bubbles, Pearls, Waves. Springer; New York: 2002.
55. Flikkema E, Bromley ST. Chemical Physics Letters. 2003; 378:622.
56. Tsuneyuki S, Tsukada M, Aoki H, Matsui Y. Physical Review Letters. 1988; 61:869. [PubMed: 10039451]
57. Vanbeest BWH, Kramer GJ, Vansanten RA. Physical Review Letters. 1990; 64:1955. [PubMed: 10041537]
58. Straatsma, TPAE.; Windus, TL.; Bylaska, EJ.; de Jong, W.; Hirata, S.; Valiev, M.; Hackler, M.; Pollack, L.; Harrison, R.; Dupuis, M.; Smith, DMA.; Nieplocha, J.; Tipparaju, V.; Krishnan, M.; Auer, AA.; Brown, E.; Cisneros, G.; Fann, G.; Früchtl, H.; Garza, J.; Hirao, K.; Kendall, R.; Nichols, J.; Tsemekhman, K.; Wolinski, K.; Anchell, J.; Bernholdt, D.; Borowski, P.; Clark, T.; Clerc, D.; Dachsel, H.; Deegan, M.; Dyall, K.; Elwood, D.; Glendening, E.; Gutowski, M.; Hess, A.; Jaffe, J.; Johnson, B.; Ju, J.; Kobayashi, R.; Kutteh, R.; Lin, Z.; Littlefield, R.; Long, X.; Meng, B.; Nakajima, T.; Niu, S.; Rosing, M.; Sandrone, G.; Stave, M.; Taylor, H.; Thomas, G.; van Lenthe, J.; Wong, A.; Zhang, Z. NW Chem, A Computational Chemistry Package for Parallel Computers. 4.6. Pacific Northwest National Laboratory; Richland, Washington: 2004.
59. Falck E, Patra M, Karttunen M, Hyvonen MT, Vattulainen I. Biophysical Journal. 2004; 87:1076. [PubMed: 15298912]
60. Leekumjorn S, Sum AK. Biophysical Journal. 2006; 90:3951. [PubMed: 16533838]
61. Knepp VM, Szoka FC, Guy RH. Journal of Controlled Release. 1990; 12:25.
62. Knepp VM, Hinz RS, Szoka FC Jr, Guy RH. Journal of Controlled Release. 1988; 5:211.
63. Hofland HEJ, Bouwstra JA, Bodde HE, Spies F, Junginger HE. British Journal of Dermatology. 1995; 132:853. [PubMed: 7662563]

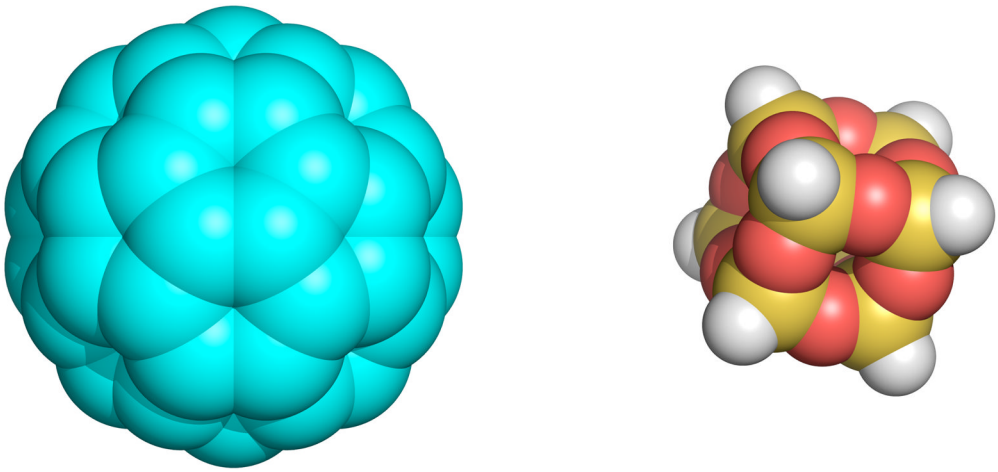

Figure 1.
C_{60} (left) and H-POSS $(SiO_{1,5})_8$ (right).

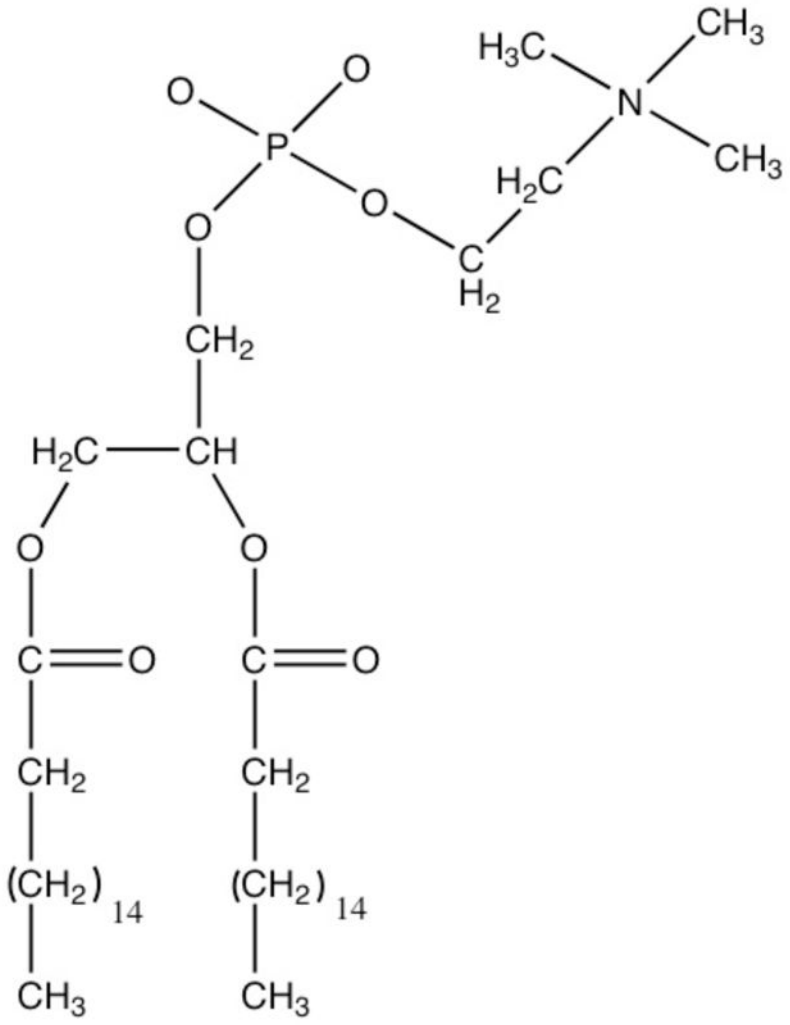

Figure 2.
Chemical structure of dipalmitoylphosphatidylcholine.

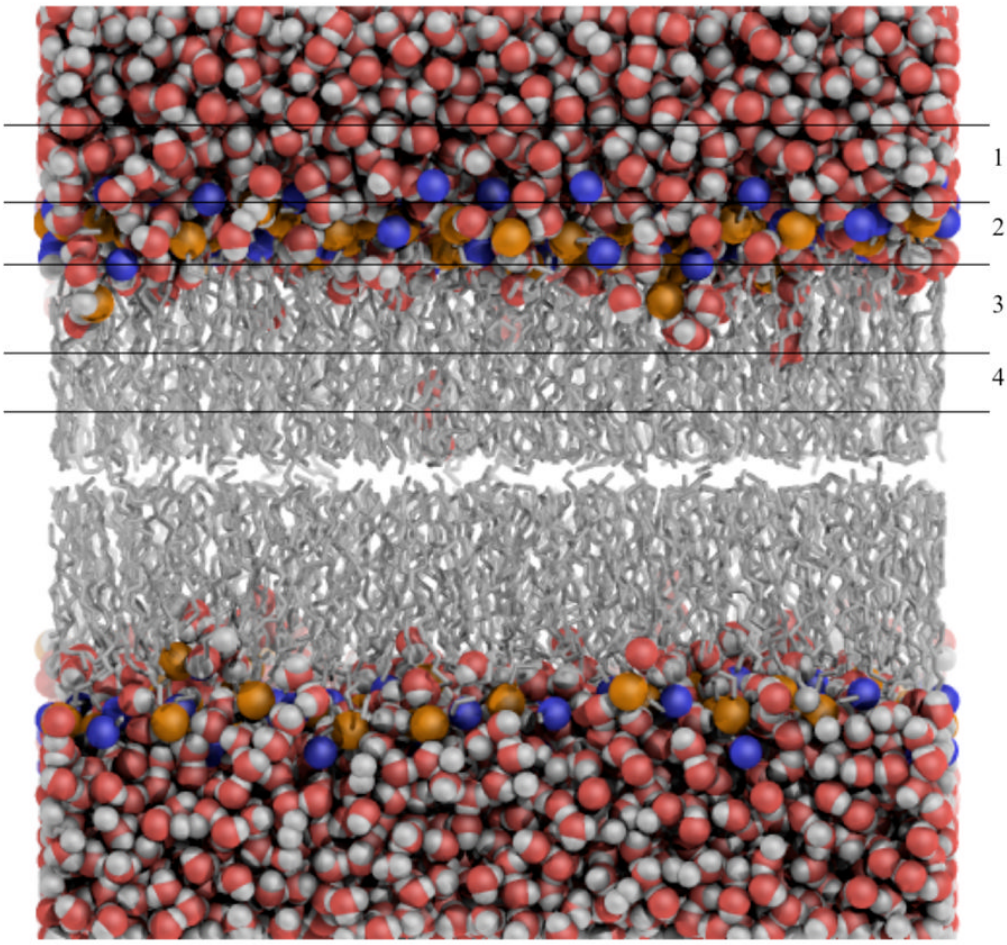

Figure 3.
The four-region model of a fully hydrated DPPC bilayer: water O (red), water H (white), nitrogen head group (blue), phosphorus head group (brown), hydrocarbon chain (grey).

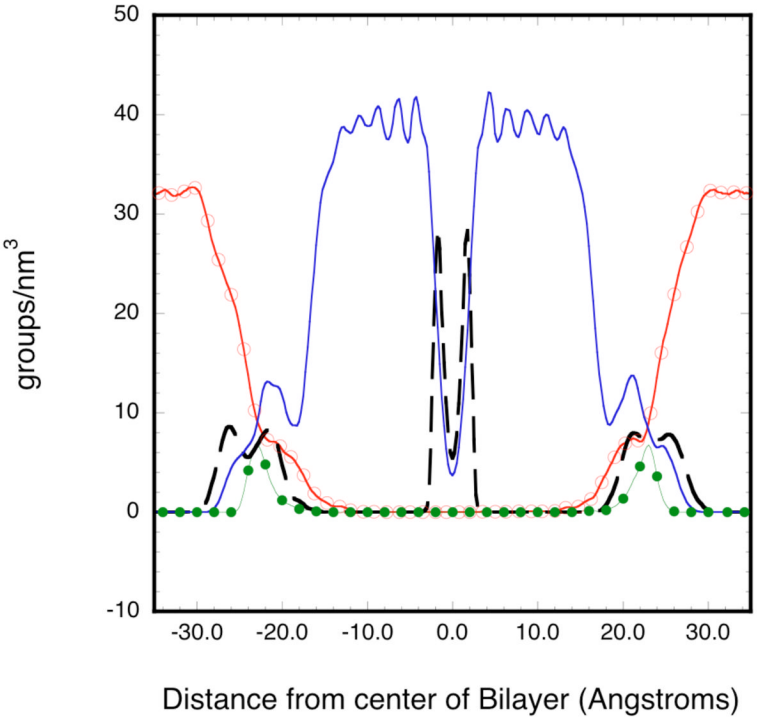

Figure 4.
Atom group densities in an unperturbed DPPC bilayer: H_2O (⊖), CH_2 (—), CH_3 (– –), and phosphrous (●).

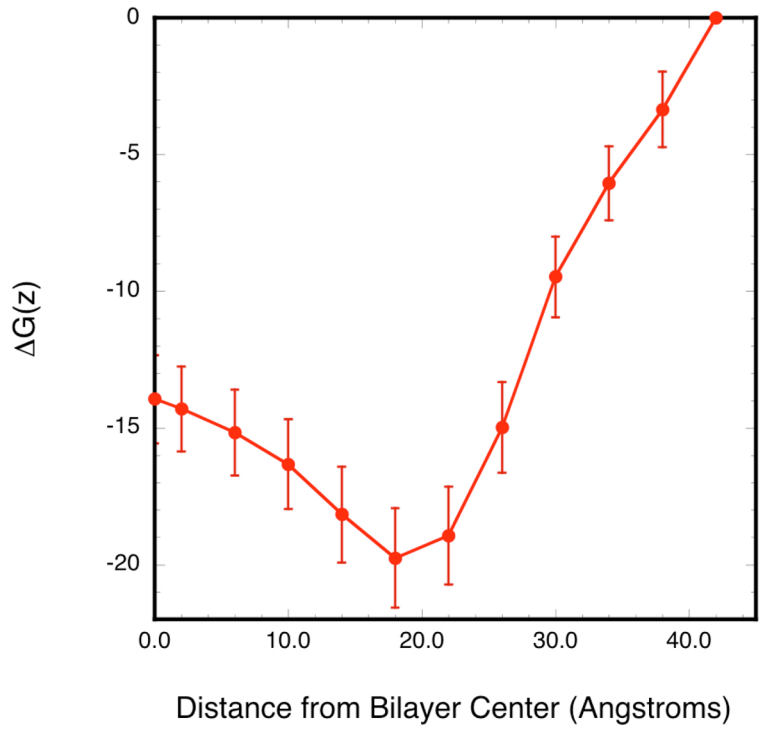

Figure 5.
$\Delta G(z)$ of C_{60} in a gel-phase DPPC bilayer.

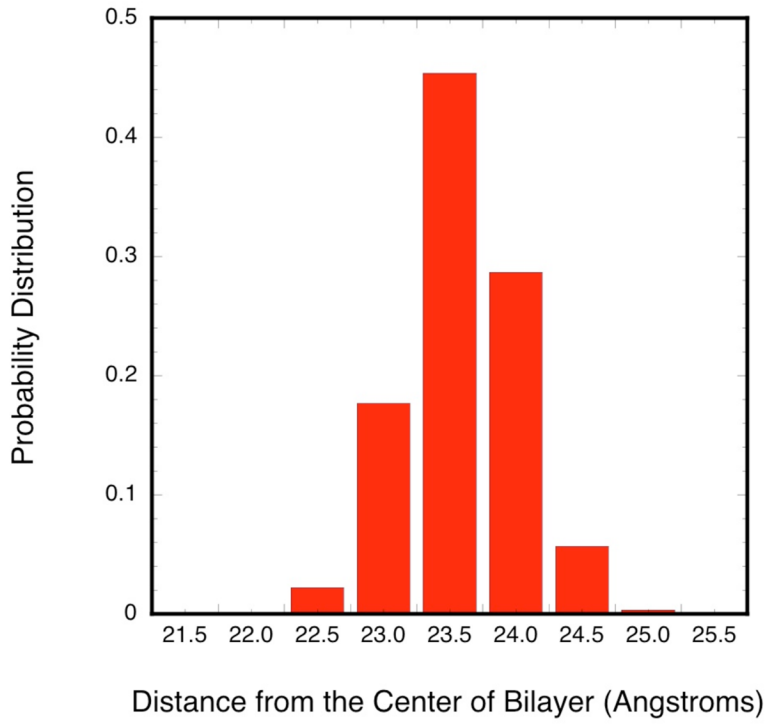

Figure 6.
Probability of finding C_{60} at various depths within the interfacial region.

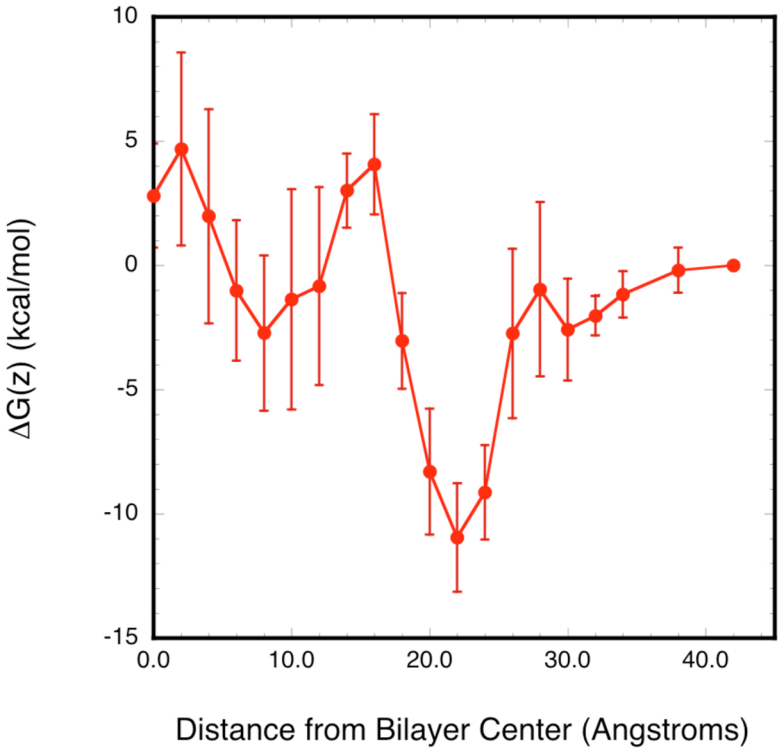

Figure 7.
Δ*G*(*z*) of H-POSS in DPPC bilayer.

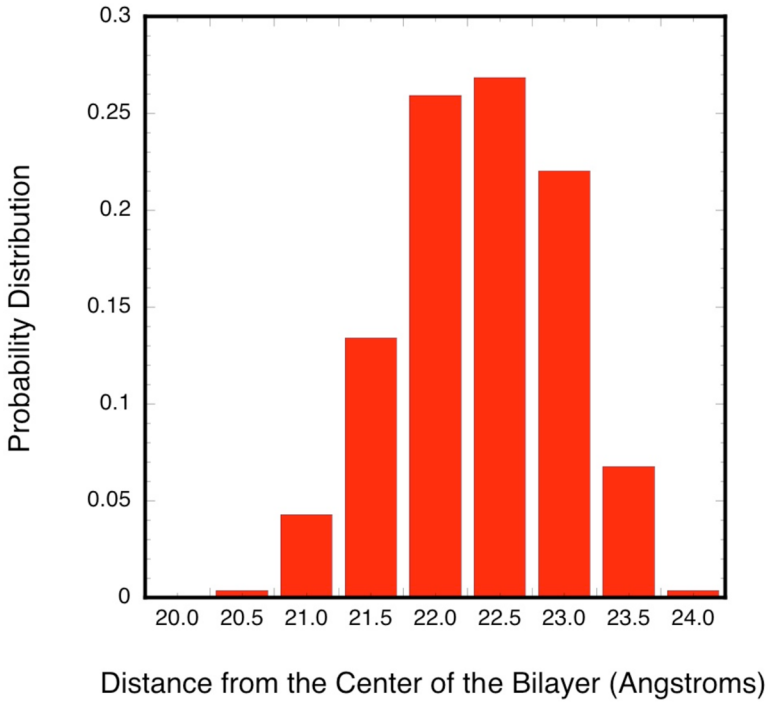

Figure 8.
Probability of finding H-POSS at various depths in the DPPC membrane.

Table 1

Results from a B3LYP-DFT/6-31G geometry optimization of H-POSS

Geometry	r_{ij} (Å)	θ_{ijk} (degrees)	φ_{ijkl} (degrees)
Si-O	1.63	-	-
Si-H	1.45	-	-
O-Si-O	-	108.97	-
Si-O-Si	-	109.47	-
H-Si-O	-	109.97	-
Si-O-Si-O	-	-	59.3
H-Si-O-Si	-	-	178.60

Table 2

Partial charges for H-POSS derived from Mulliken population analysis

Atom	q_i
Si	1.83
O	−1.15
H	0.105